Original Article

IRISIN LIPOSOMES INHIBIT FERROPTOSIS AND IMPROVE ATHEROSCLEROSIS IN MOUSE MODELS VIA THE NRF2/HO-1 SIGNALING PATHWAY

Z. Han[1,2,§], Y.R. Lan[3,§], B. Yuan[2] and Q.L. Chen[4,*]

[1]Institute of Medical Engineering and Translational Medicine, Tianjin University, 300072 Tianjin, China
[2]Department of Neurology, Hebei University Affiliated Hospital, 071030 Baoding, Hebei, China
[3]Graduate School of Tianjin Medical University, Tianjin Medical University, 300070 Tianjin, China
[4]Department of Cardiac Surgery, Tianjin Chest Hospital, 300222 Tianjin, China
[§]These authors contributed equally.

Abstract

Background: Atherosclerosis (AS)—a chronic arterial wall inflammation driven by lipid dysmetabolism—progresses through oxidative stress and inflammatory cascades. Ferroptosis is established as a pivotal pathogenic driver in AS. Here, we leverage exercise-induced cytokine irisin, delivered via liposomal carriers, to therapeutically suppress ferroptotic signaling and ameliorate atherosclerotic pathogenesis. **Methods:** Irisin liposomes were prepared using the complex emulsion method, and a suitable concentration of irisin was determined using the Cell Counting Kit-8 (CCK-8) method. A vascular endothelial cell injury model was constructed to investigate the protective effect of irisin liposomes on vascular endothelial cells using apoptosis detection, lactate dehydrogenase (LDH) detection, mitochondrial membrane potential detection, and transmission electron microscopy morphology detection. The expression levels of key genes in the nuclear factor erythroid 2-related factor 2 (Nrf2)/heme oxygenase-1 (HO-1) signaling pathway were detected using western blotting and quantitative real-time polymerase chain reaction (qRT-PCR). A mouse model of atherosclerosis was constructed, and irisin liposomes were administered via tail vein injection to treat the mice. Serum levels of total cholesterol (TC), triglyceride (TG), low-density lipoprotein cholesterol (LDL-C), high-density lipoprotein cholesterol (HDL-C), oxidized low-density lipoprotein (ox-LDL), reactive oxygen species (ROS), and Fe^{2+} were detected by kits, and levels of malondialdehyde (MDA), glutathione (GSH), superoxide dismutase (SOD), oxidized glutathione (GSSG), and 4-hydroxynonenal (4-HNE) were detected by enzyme-linked immunosorbent assay (ELISA). Hematoxylin and eosin (H&E) staining and alizarin red staining were used to detect carotid artery tissues pathologically. ELISA, immunohistochemistry, western blot, and qRT-PCR were used to detect the expression levels of key genes in the Nrf2/HO-1 signaling pathway in carotid artery tissues. **Results:** The umbilical vein endothelial cells maintained high activity at an irisin concentration of 25 nmol/L. By comparing the apoptosis, cytotoxicity, and mitochondrial morphology and membrane potential changes in the blank serum group, vascular endothelial cell injury model group, and irisin group, the irisin liposome group had a better function of protecting vascular endothelial cells and activated the Nrf2/HO-1 signaling pathway. In the atherosclerosis mouse model, the irisin liposome group significantly downregulated the levels of TC, TG, LDL-C, and ox-LDL and upregulated the level of HDL-C. The irisin liposome group significantly downregulated the levels of Fe^{2+}, MDA, ROS, GSSG, and 4-HNE and upregulated the levels of GSH, SOD, and irisin, which are indicators related to the ferroptosis. Simultaneously, it improved the pathology in the carotid artery tissues of atherosclerotic mice, mainly by activating the Nrf2/HO-1 signaling pathway, upregulating the levels of Nrf2, HO-1, glutathione peroxidase 4 (GPX4), and solute carrier family 7 member 11 (SLC7A11), and downregulating the expression levels of acyl-CoA synthetase long chain family member 4 (ACSL4) and tumor protein 53 (P53). **Conclusions:** Irisin liposomes exerted enhanced protective effects on vascular endothelial cells, inhibited ferroptosis by activating the Nrf2/HO-1 signaling pathway, and ameliorated damage in a mouse model of AS, which had a therapeutic effect on AS.

Keywords: Cardiovascular disease, Nrf2/HO-1, irisin liposomes, ferroptosis.

***Address for correspondence**: Q.L. Chen, Department of Cardiac Surgery, Tianjin Chest Hospital, 300222 Tianjin, China. Email: tjdxygyhz@163.com.

Introduction

Cardiovascular disease (CVD) is a common disease that seriously jeopardizes human life and health [1]. According to statistics, the incidence and mortality rate of cardiovascular disease are the highest. In 2019, more than 17.9 million people died worldwide from CVD, accounting for more than 32 % of global deaths [2]. Atherosclerosis (AS) serves as the cornerstone of cardiovascular disease and is marked by lipid metabolic disorders along with endothelial dysfunction [3]. Lipids in the plasma are essential for the basal metabolism of living cells. Dyslipidemia acts as an autonomous contributor to cardiovascular pathogenesis within atherosclerotic progression [4]. The lipid components that are often measured are total cholesterol (TC), triglycerides (TGs), low-density lipoprotein (LDL) cholesterol, and high-density lipoprotein (HDL). Elevated levels of LDL lead to plaque formation in the arterial wall, which can lead to atherosclerosis [5]. The pathogenesis of atherosclerosis is complex, and current treatment for atherosclerosis is still based on antiplatelet and anti-inflammatory drugs [6]. Therefore, there is a need to identify more efficient therapeutic agents.

Irisin, an exercise-responsive polypeptide chain of 112 amino acids (112-aa) myokine proteolytically cleaved from skeletal muscle fibronectin type III domain-containing protein 5 (FNDC5), coordinates inter-tissue metabolic crosstalk [7]. Exercise is the primary stimulus for irisin production [8]. Peroxisome proliferator-activated receptor gamma coactivator 1-alpha (PGC-1α) acts as the master transcriptional regulator of irisin biogenesis by directly activating FNDC5 enhancer-promoter complexes, followed by proteolytic processing of the FNDC5 precursor protein to yield functional irisin [9]. Irisin promotes heat production by activating the uncoupling protein 1 (UCP1) in the mitogen-activated protein kinase (MAPK)/extracellular signal-regulated kinase (ERK) pathway, thereby regulating browning of white adipose tissue [10,11]. Several studies have demonstrated the role of irisin in improving atherosclerosis [12,13]. A recent study has shown that FNDC5 can improve atherosclerosis by inhibiting NOD-like receptor family pyrin domain-containing protein 3 (NLRP3) expression and attenuating oxidized low-density lipoprotein (ox-LDL)-induced smooth muscle-derived foam cell formation and monocyte adhesion [14]. Irisin stimulates nitric oxide (NO) secretion from endothelial cells and promotes vasodilation in animal models of hyperglycemia and hypertension [15]. Irisin therapy rescued apoptosis-compromised plaque cells, suppressed macrophage infiltration, and repressed pro-inflammatory cytokine production in atherosclerotic lesions of murine models [16]. Liposomal drug delivery systems have attracted much attention from researchers because of their advantages such as high efficiency, low toxicity, targeting, and controlled release of drugs [17]. Liposomes are delivery systems consisting of natural or synthetic solid lipids (e.g., lecithin and triglycerides) with particle sizes ranging from 10 to 1000 nm [18]. The drug is encapsulated or embedded in a lipid core, which combines the advantages of both liposomes and particles (LPs), making it an ideal drug delivery system [19].

Oxidative stress is one of the most important factors involved in the pathology of atherosclerosis [20]. Reactive oxygen species (ROS) are produced by oxygen reduction and are a group of reactive molecules that regulate various cellular functions and biological processes [21]. On the one hand, a moderate amount of ROS maintains vascular homeostasis, while on the other hand, excessive ROS cause vascular damage [20]. ROS play an important role in cell growth and apoptosis, inflammatory and alterations in vascular tone, as well as in the production of oxidized LDL [22]. Reactive oxygen species (ROS) drive atherosclerotic pathogenesis through a triad of interconnected pathways: (1) oxidative damage to cellular lipids and genomic DNA, (2) disruption of endothelial homeostasis, (3) and initiation of pro-inflammatory cascades [23]. ROS also affect plaque stability by upregulating the expression and enhancing the activity of matrix metalloproteinases (MMP) [24]. Atherosclerotic progression is mechanistically linked to iron dyshomeostasis. Elevated cytosolic Fe^{2+} levels, arising from genetic or metabolic insults, catalyze hydroxyl radical (•OH) formation via the Fenton reaction, resulting in ROS burst that executes ferroptotic cell death and plaque destabilization [25]. Ferroptosis is a recently defined programmed modality of cell death, characterized by intracellular labile iron overload and lipid peroxidation [26]. Inhibition of ferroptosis has been demonstrated to reduce ox-LDL levels and atherosclerotic plaques and delay atherosclerotic progression in *ApoE*-deficient mice [27]. In high-fat diet-induced $ApoE^{-/-}$ mice, ferretin-1 (Fer-1) attenuated atherosclerosis by reducing iron accumulation and lipid peroxidation, suggesting a role for ferroptosis in atherosclerosis [27].

Activation of the nuclear factor erythroid 2-related factor 2 (Nrf2)/heme oxygenase-1 (HO-1) pathway is pivotal in suppressing ROS-driven inflammation and maintaining oxidative balance [28]. As a central transcriptional coordinator, Nrf2 governs the expression of antioxidant genes and modulates signaling networks underlying diverse cytoprotective responses [29]. HO-1 has many important roles in protecting against atherosclerosis, including antioxidant, anti-inflammatory, and anti-apoptotic activities [30]. HO-1 is a target protein downstream of Nrf2, and several studies have demonstrated an inhibitory effect of the Nrf2/HO-1 axis on ferroptosis [31,32].

Based on the therapeutic effects of irisin on atherosclerosis, we investigated the potential mechanism of irisin against oxidative stress. In this study, we evaluated the therapeutic effects of liposome-encapsulated irisin on atherosclerosis by constructing vascular endothelial cell injury and mouse models of atherosclerosis. The primary fo-

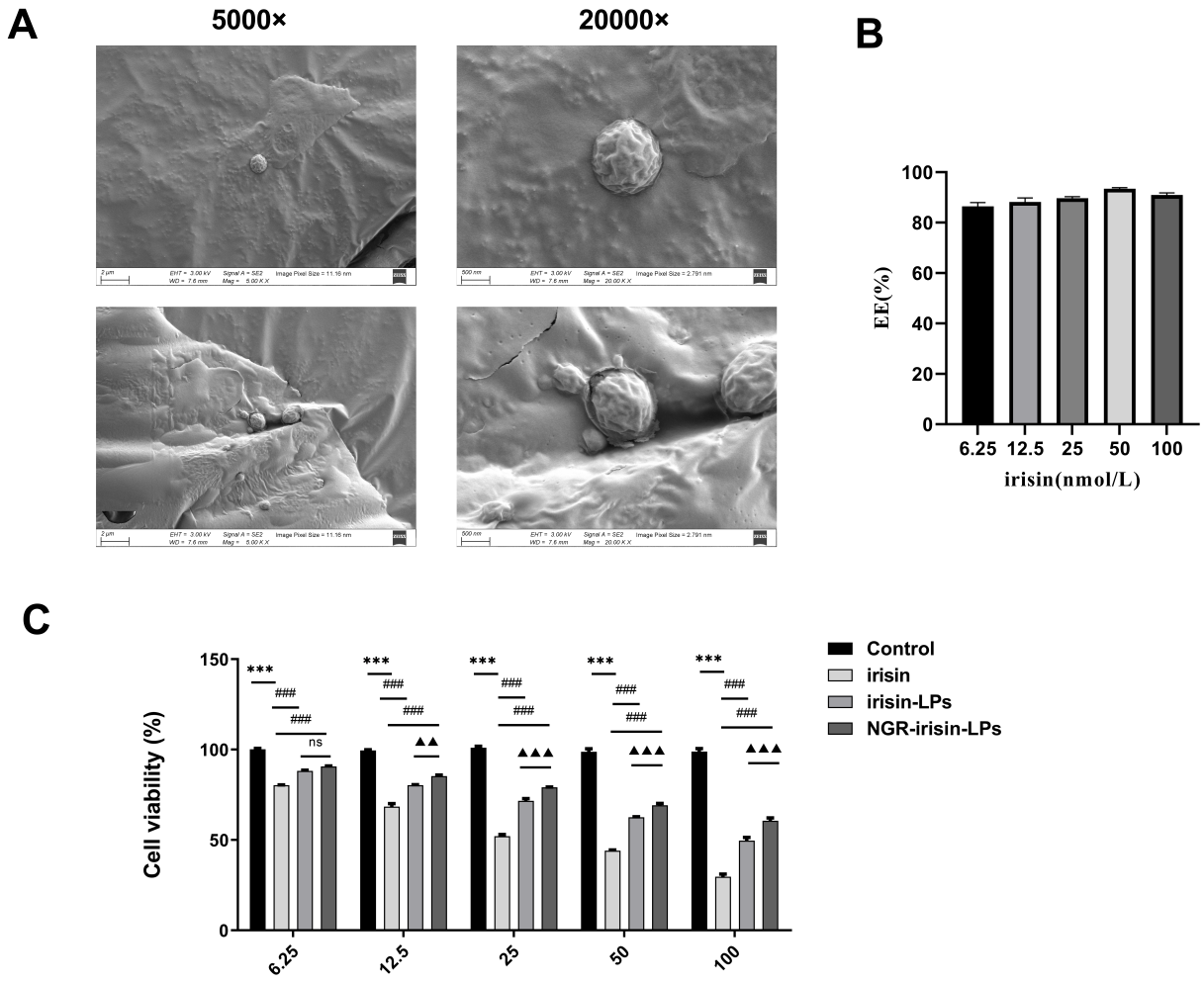

Fig. 1. Construction of irisin encapsulated in liposomes and determination of the appropriate irisin concentration. (**A**) Scanning electron microscope observation of liposome particle size (n = 6). Scale bars are 2 μm and 500 nm. (**B**) Encapsulation rates of liposomes with different concentrations of irisin (n = 6). (**C**) CCK-8 assay of umbilical vein endothelial cell activity after treatment with different irisin concentrations (n = 6). Based on control group, $^{***}p < 0.001$; based on irisin group, $^{\#\#\#}p < 0.001$; based on Irisin-LP group, $^{\blacktriangle\blacktriangle}p < 0.01$, $^{\blacktriangle\blacktriangle\blacktriangle}p < 0.001$; ns, not significant; CCK-8, Cell Counting Kit-8; Irisin-LP, irisin liposomes; NGR, Asn-Gly-Arg peptide; EHT, extra-high tension; WD, working distance: Mag, magnification; EE % = (amount of irisin entrapped/total irisin added) × 100 (Image courtesy of GraphPad Prism 9.0.0).

cus of this study was to determine whether irisin could activate the Nrf2/HO-1 signaling pathway, inhibit the occurrence of ferroptosis in vascular endothelial cells, and ameliorate atherosclerotic effects.

Materials and Methods

Preparation and Electron Microscopic Observation of Irisin Liposomes

In this study, two types of irisin-loaded liposomes were prepared: non-targeted irisin liposomes (Irisin-LP) and Asn-Gly-Arg peptide (targeting sequence) (NGR)-modified irisin liposomes (NGR-Irisin-LP). Lecithin (F20090004; Lipoid GmbH, Ludwigshafen, Germany) and cholesterol (C8667; Merck, St. Louis, MO, USA) were proportionally mixed and dissolved in chloroform to obtain a liquid solution. An irisin (SRP8039; Merck, St. Louis, MO, USA) solution was added, and the mixture was sonicated (300 W, 5 min) to form a W/O emulsion, wherein the aqueous (W) irisin solution was dispersed as fine droplets within the continuous organic (O) chloroform phase. Ultrapure water was then added, and the mixture was sonicated for 5 min to form a W/O/W-type emulsion, which is a double emulsion structure consisting of smaller water-in-oil droplets themselves dispersed within a continuous external water phase. Liposome suspension was obtained by hydration at 30 °C and filtration through a filter membrane with a pore size of 0.45 μm. Asn-Gly-Arg (NGR)-irisin liposomes were prepared using the complex emulsion method, and the targeting components DSPE-mPEG2000-COOH

(1,2-distearoyl-sn-glycero-3-phosphoethanolamine-N-[methoxy(polyethylene glycol)-2000]-carboxylic acid), a phospholipid-polymer conjugate that serves as the backbone for coupling targeting ligands and extends liposome circulation time, and NGR-DSPE-mPEG2000, the active targeting component where the NGR peptide is covalently linked to DSPE-mPEG2000 to direct the liposomes to tissues expressing the target receptor (e.g., cluster of differentiation 13 (CD13)), were added during the preparation process to prepare NGR-Irisin-LP. The Irisin-LP were glued to the sample tray using a conductive adhesive, and the samples were placed in the chamber of the gold sprayer and sprayed with gold for 10 s. For morphological analysis, liposomes were sputter-coated with gold for 10 s and visualized under a scanning electron microscope (TM4000II; Hitachi, Ibaraki, Japan) at 15 kV accelerating voltage and 10 mm working distance.

Measurement of Optical Density (OD) Value and Encapsulation Rate

Different concentrations (6.25, 12.5, 25, 50, and 100 nmol/L) of irisin solution were prepared in phosphate-buffered saline (PBS) (pH 7.0) and scanned using a UV spectrophotometer (Nanodrop 2000; ThermoFisher, Waltham, MA, USA) to determine the best absorption peak. Different concentrations of irisin solution were prepared, the OD value was measured using an enzyme meter, and the standard curve of irisin was constructed. A certain amount of 10 % Trilatone X-100 (648463; Merck, St. Louis, MO, USA) was added to the corresponding concentrations of the drug liposome samples. The liposomes were cleaved, the encapsulated drug was released, and the concentration of the encapsulated drug was determined. After separating the liposome from the free drug, the irisin content was determined separately, the amount of encapsulated drug and free drug was calculated from the standard curve, and the encapsulation rate was calculated.

Cell Culture and Treatment

Human umbilical vein endothelial cell lines (HUVECs, TCH-C406) were purchased from Procell Life Science & Technology (Wuhan, China). The cells were confirmed free of mycoplasma contamination using polymerase chain reaction (PCR) assay and were authenticated by short tandem repeat (STR) profiling (**Supplementary Fig. 1**). The cells were cultured in 1640 medium from Gibco (31800-022; Grand Island, NY, USA) supplemented with 10 % fetal bovine serum (FBS) from Gibco (A5256701; Grand Island, NY, USA) and 100 units/mL penicillin/streptomycin from Sigma (15140-122; St. Louis, MO, USA). We maintained the cells at 37 °C in a humidified incubator containing 5 % CO_2. For experiments, cells were allocated into five groups (n = 6 replicates per group): blank group: No drug treatment; model group: HUVEC induced with H_2O_2 (2.0 mmol/L) for 4 h; irisin group: Pretreated with free irisin (25 nmol/L) for 24 h before H_2O_2 induction; Irisin-LP group: Pretreated with non-targeted irisin liposomes (25 nmol/L) for 24 h before H_2O_2 induction; NGR-Irisin-LP group: Pretreated with NGR-targeted irisin liposomes (25 nmol/L) for 24 h before H_2O_2 induction.

Treatments were assigned to wells in a randomized order using a computer-generated sequence (Excel (Version of Microsoft 365; Microsoft Corporation, Redmond, WA, USA) RAND function) to minimize plate position bias. Irisin was dissolved in dimethyl sulfoxide (DMSO) (472301; Merck, St. Louis, MO, USA).

Cell Viability Assay

In 96-well plates, HUVEC cells were inoculated at a density of 2000 cells per well, and the cells were treated by different concentrations (6.25, 12.5, 25, 50, and 100 nmol/L) of irisin, Irisin-LP group, NGR-Irisin-LP group, and blank group. The cells were incubated in medium supplemented with 10 % FBS at 37 °C for 48 h. After the incubation period, 10 μL of Cell Counting Kit-8 (CCK-8) solution from Bioss (BA00208; Beijing, China) was added to each well, along with 100 μL of medium. The cells were incubated for an additional 4 h at 37 °C, and the OD value at 450 nm was measured using an RT-6000 enzyme microplate reader from Rayto Life and Analytical Sciences Co., Ltd. (Shenzhen, China).

Lactate Dehydrogenase (LDH) Detection

The working solution A (1200 μL) was prepared according to the instructions of the kit (ab102526; Abcam, Cambridge, UK). The cell culture plate was removed, and the culture solution from each well was transferred to a centrifuge tube, centrifuged at 1000 rpm for 3 min. Then, 120 μL of the supernatant and 60 μL of the working solution were evenly dispensed into each well of the 96-well plate. The plate was incubated at room temperature and avoiding light for 30 min. Then, the absorbance was measured using an enzyme meter at 490 nm.

Mitochondrial Membrane Potential and Morphology Assay

The treated HUVEC were harvested and resuspended in 0.5 mL cell culture solution. JC-1 staining working solution (0.5 mL, ab113850; Abcam, Cambridge, UK) was added in cell culture solution, and the cells were incubated at 37 °C for 20 min. Subsequently, 1 mL of JC-1 staining buffer was added in cell culture solution, and the samples were analyzed using flow cytometry (Attune NxT, Abcam, Cambridge, UK). Cells were collected for low-temperature agar pre-embedding, subjected to fixation, dehydration, embedding, resin polymerization, ultrathin sectioning, and staining, and were observed and photographed using a transmission electron microscope (HT7700; Hitachi, Tokyo, Japan).

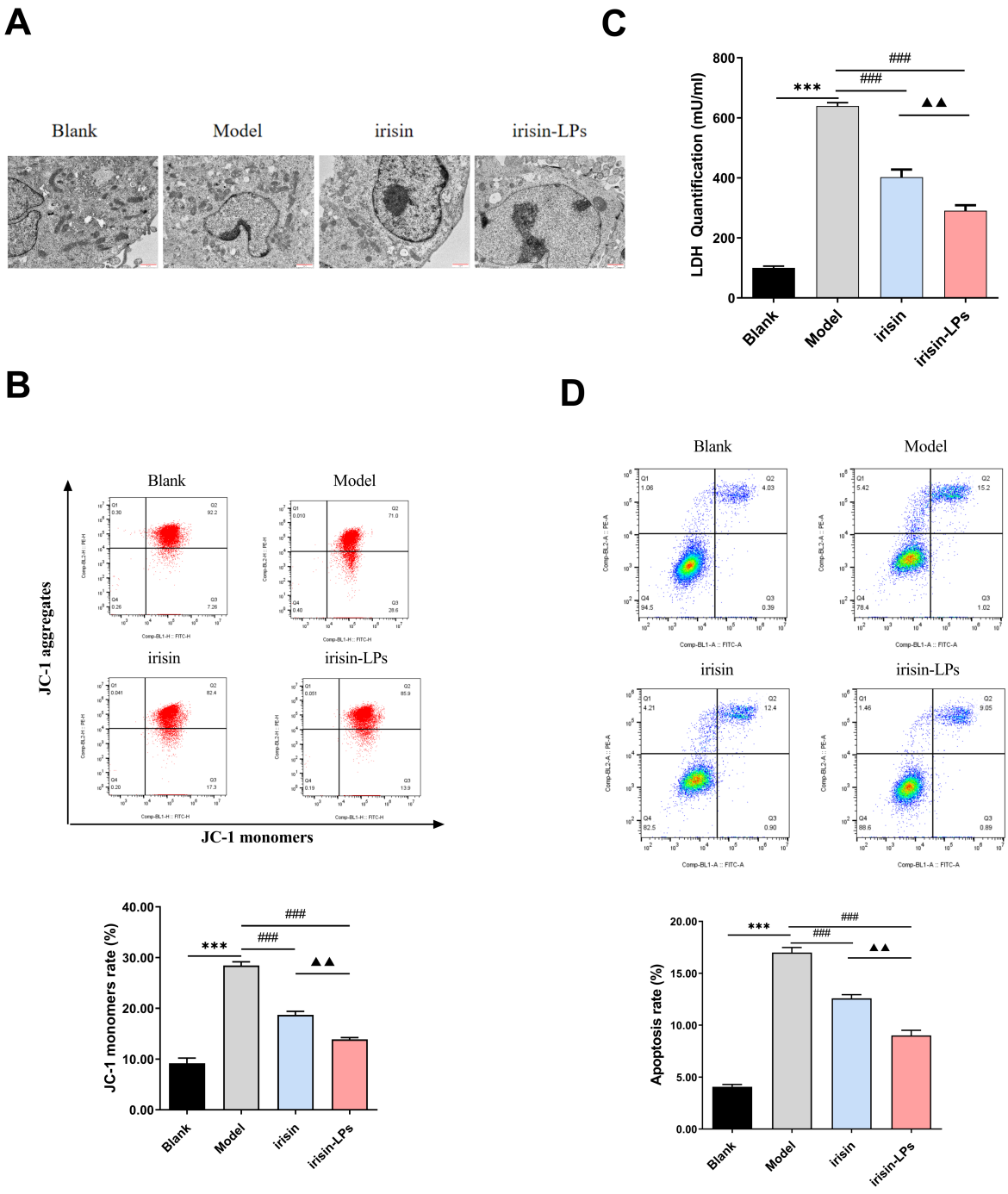

Fig. 2. Assessment of the effect of irisin liposomes on a vascular endothelial cell injury model. (**A**) Transmission electron microscopy was used to detect morphological changes in mitochondria (n = 6). Scale bars are 1 μm. (**B**) JC-1 probe was used to detect the mitochondrial membrane potential (n = 6). (**C**) Cytotoxicity was detected by the LDH assay (n = 6). (**D**) Flow cytometry was used to detect cell apoptosis (n = 6). Based on blank group, $^{***}p < 0.001$; based on model group, $^{\#\#\#}p < 0.001$; based on irisin group, $^{\blacktriangle\blacktriangle}p < 0.01$; LDH, lactate dehydrogenase; JC-1, 5,5′,6,6′-tetrachloro-1,1′,3,3′-tetraethylbenzimidazolyl-carbocyanine iodide; FITC, fluorescein isothiocyanate (Image courtesy of GraphPad Prism 9.0.0).

Western Blot

The total protein was extracted using a 5–12 % sodium dodecyl sulfate-polyacrylamide gel electrophoresis (SDS-PAGE) gel, which was subsequently transferred onto a polyvinylidene difluoride (PVDF) membrane. The membrane was blocked with 5 % skimmed milk at 25 °C for 1 h. Following this, the membrane was incu-

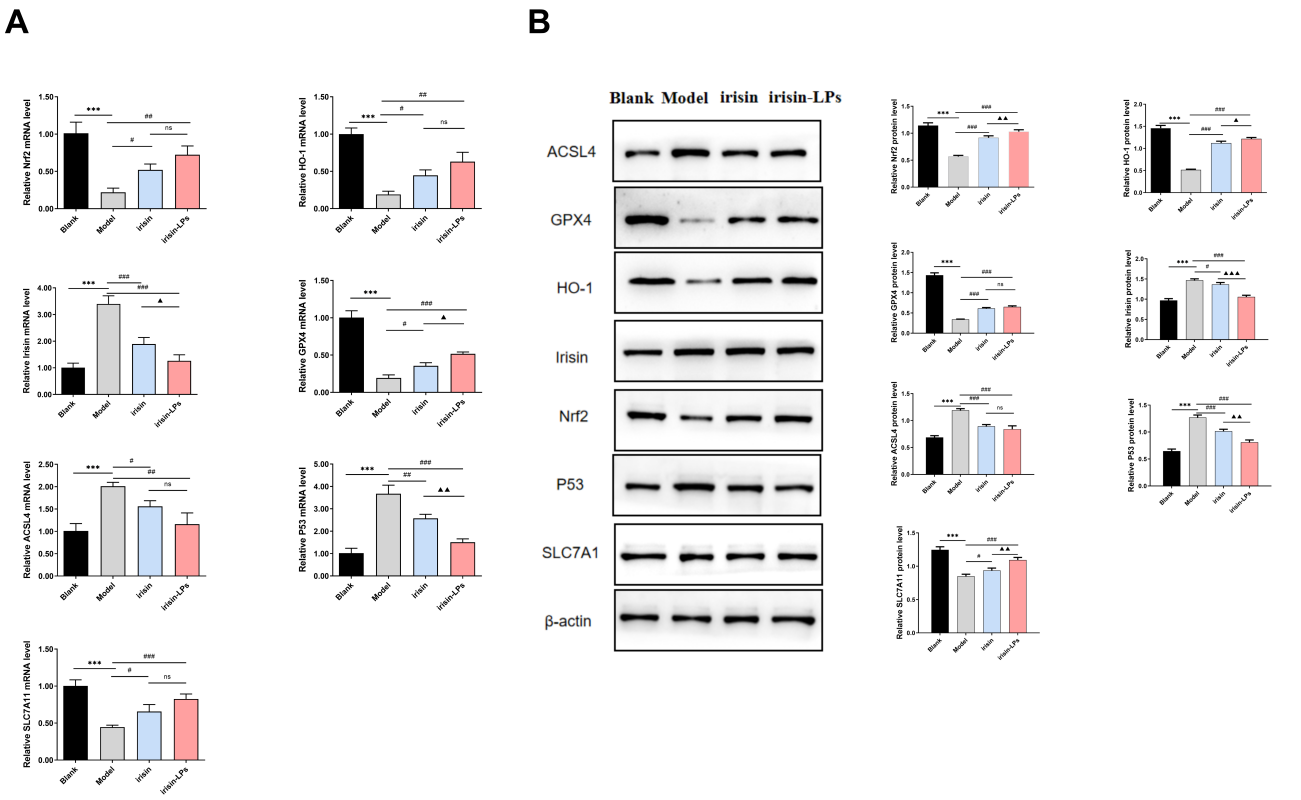

Fig. 3. Detection of Nrf2/HO-1 signaling pathway activation by irisin liposomes in a vascular endothelial cell injury model. (**A**) qRT-PCR was used to detect the expression level of mRNA of *Nrf2/HO-1* axis related genes in vascular endothelial cells (n = 6). (**B**) Western blot was used to detect the expression level of Nrf2/HO-1 axis related proteins in vascular endothelial cells (n = 6). Based on blank group, $^{***}p < 0.001$; based on model group, $^{\#}p < 0.05$, $^{\#\#}p < 0.01$, $^{\#\#\#}p < 0.001$; based on irisin group, $^{\blacktriangle}p < 0.05$, $^{\blacktriangle\blacktriangle}p < 0.01$, $^{\blacktriangle\blacktriangle\blacktriangle}p < 0.001$; ns, not significant; Nrf2, nuclear factor erythroid 2-related factor 2; HO-1, heme oxygenase-1; qRT-PCR, quantitative real-time polymerase chain reaction; GPX4, glutathione peroxidase 4; ACSL4, acyl-CoA synthetase long chain family member 4; P53, tumor protein 53; SLC7A11, solute carrier family 7 member 11; mRNA, messenger RNA (Image courtesy of GraphPad Prism 9.0.0).

bated overnight at 4 °C with the primary antibody acyl-CoA synthetase long chain family member 4 (ACSL4) (ab155282), glutathione peroxidase 4 (GPX4) (ab125066), HO-1(ab52947), irisin (ab174833), Nrf2 (ab62352), tumor protein 53 (P53) (ab32049), solute carrier family 7 member 11 (SLC7A11) (ab307601), β-actin (ab8227) (Abcam, Cambridge, MA, USA), and then with the secondary antibody for 1 h at room temperature. The chemiluminescence reagents were mixed in equal volumes of liquid A and liquid B (P10100; NCM Biotech, Suzhou, China). The membranes were incubated for 5 min and then detected by JP-K6000 chemiluminescence imager (Jiapeng, Shanghai, China). Protein expression was analyzed using ImageJ software (version 1.8.0; NIH, Bethesda, MD, USA) for optical density values.

Quantitative Real-Time Polymerase Chain Reaction (qRT-PCR)

Total RNA was isolated using Cell/Tissue Total RNA Isolation Kit V2 (RC112-01; Vazyme, Nanjing, China) according to the manufacturer's protocol. Total RNA was reverse transcribed into complementary DNA (cDNA) using HiScript lll 1st Strand cDNA Synthesis Kit (R312-01; Vazyme, Nanjing, China). qRT-PCR was performed using CFX96 Touch 1855195 (Bio-Rad, Hercules, CA, USA) with Taq Pro Universal SYBR qPCR Master Mix (Q712; Vazyme, Nanjing, China). Each sample underwent triplicate analysis, with glyceraldehyde-3-phosphate dehydrogenase (GAPDH) serving as the reference. Quantitative results were determined using the 2-ΔΔCT method. The primers (Lot No.: SO20231108A) utilized for qRT-PCR were designed and synthesized by Sangon Biotech (Shanghai, China) (Table 1).

Animal Models and Therapeutic Subgroups

The mouse atherosclerosis model was constructed using 45 male *ApoE*$^{-}$/$^{-}$ mice (8–10 weeks old, body weight 20–25 g). Mice were randomly divided into three groups (n = 9 per group) via a computer-generated randomization sequence (GraphPad Prism v9.0; San Diego, CA, USA): control group: Fed normal chow (D12108; Research Diets, New Brunswick, NJ, USA) and injected with 200 μL saline

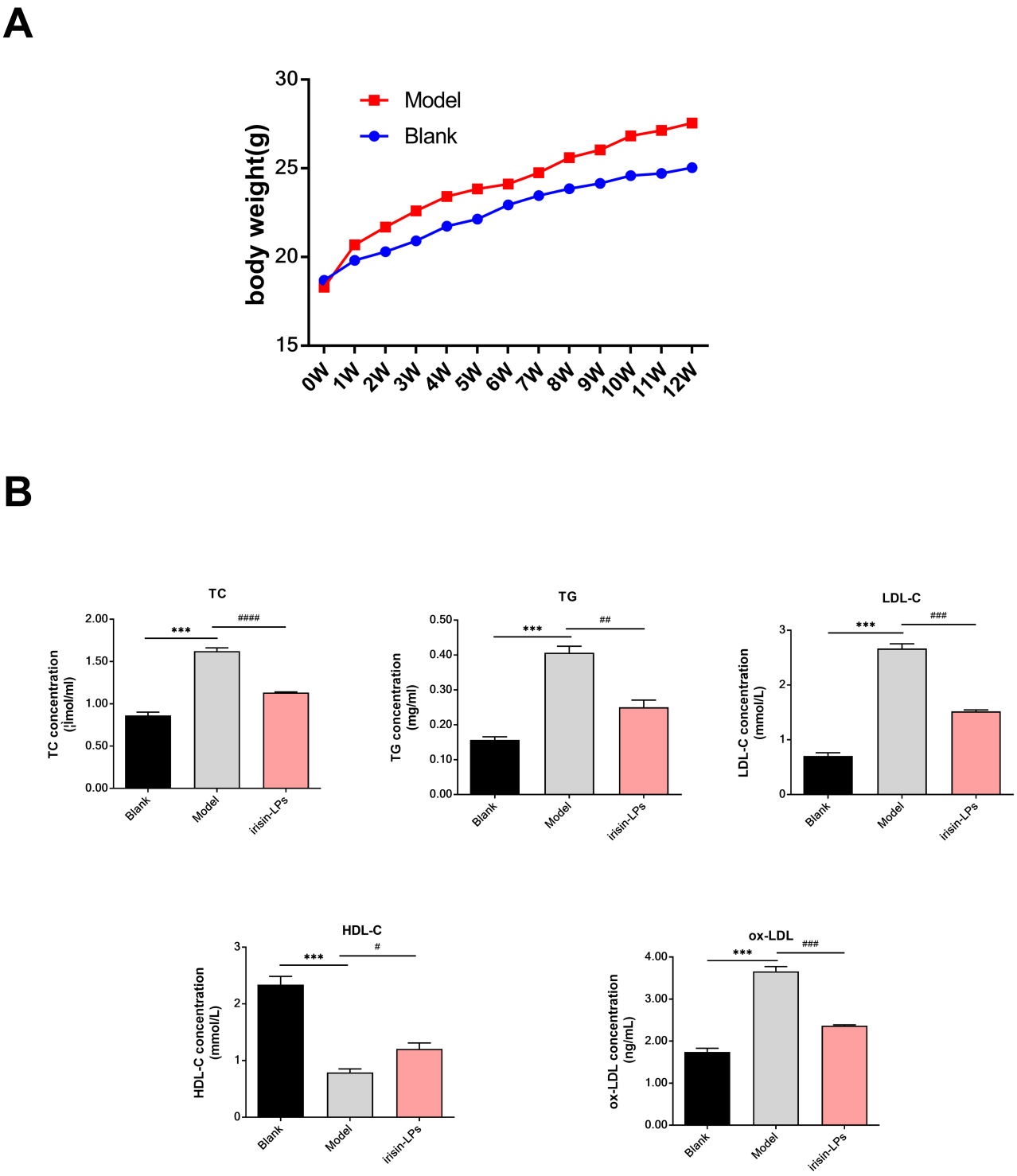

Fig. 4. Detection of lipid levels of irisin liposomes on atherosclerosis model mice. (**A**) Body weight changes in atherosclerosis model mice (n = 9). (**B**) Detection of serum levels of TC, TG, LDL-C, HDL-C, and ox-LDL after irisin liposomes treatment in atherosclerosis model mice (n = 9). Based on blank group, $^{***}p < 0.001$; based on model group, $^{\#}p < 0.05$, $^{\#\#}p < 0.01$, $^{\#\#\#}p < 0.001$, $^{\#\#\#\#}p < 0.001$; TC, total cholesterol; TG, triglyceride; LDL-C, low-density lipoprotein cholesterol; HDL-C, high-density lipoprotein cholesterol; ox-LDL, oxidized low-density lipoprotein (Image courtesy of Graphpad Prism 9.0.0).

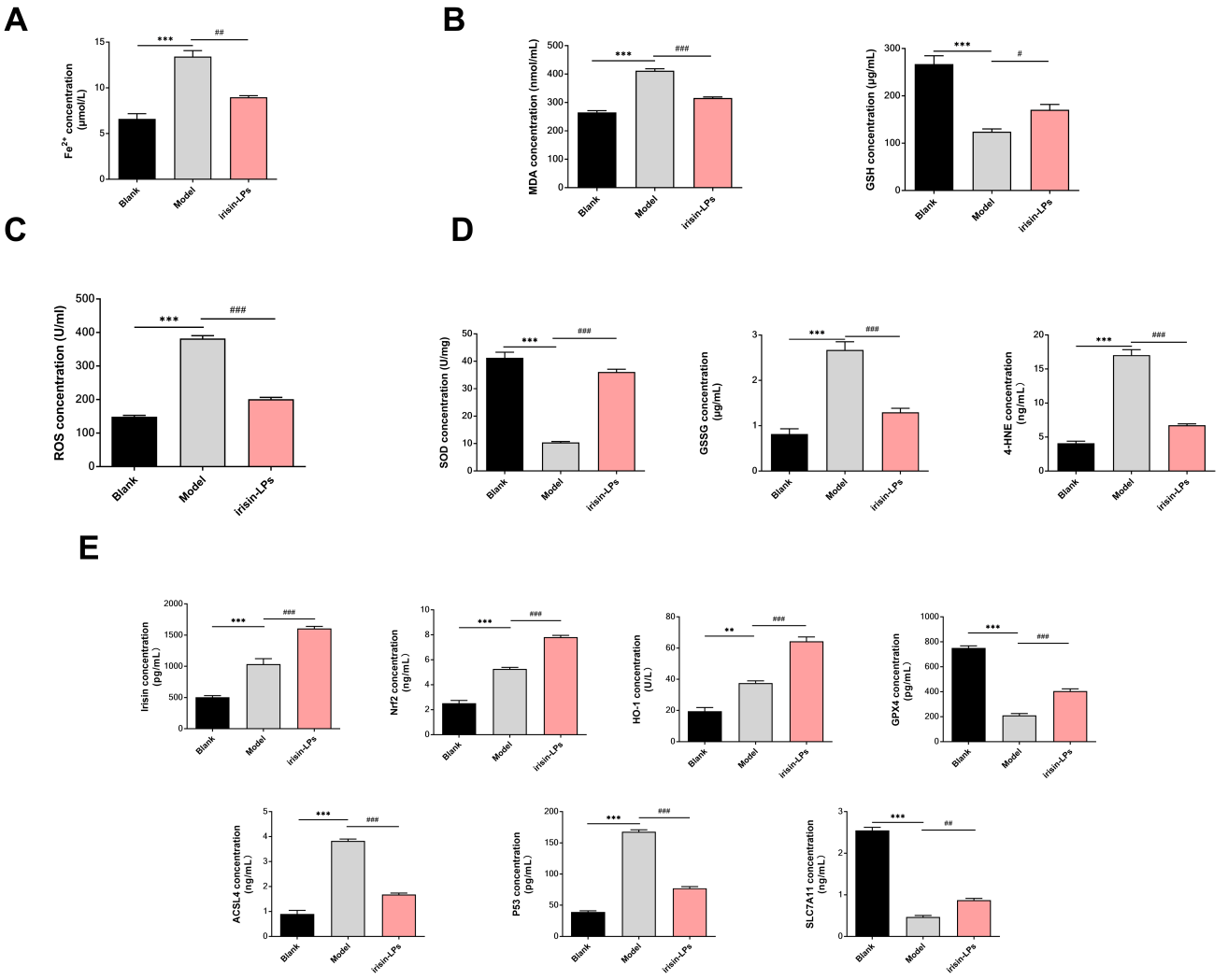

Fig. 5. Detection of the regulatory effects of irisin liposomes on ferroptosis in an atherosclerosis mouse model. (**A**) Fe^{2+} kit detects the level of Fe^{2+} in the carotid artery tissues (n = 6). (**B**) MDA and GSH assay kit detects the level of MDA and GSH in carotid artery tissues (n = 6). (**C**) ROS assay kit detects the level of ROS in carotid artery tissues (n = 6). (**D**) ELISA was used to detect the levels of SOD, GSSG, and 4-HNE in carotid artery tissues (n = 6). (**E**) ELISA was used to detect the expression level of Nrf2/HO-1 axis-related protein (n = 6). Based on blank group, $^{**}p < 0.01$, $^{***}p < 0.001$; based on model group, $^{\#}p < 0.05$, $^{\#\#}p < 0.01$, $^{\#\#\#}p < 0.001$; MDA, malondialdehyde; GSH, glutathione; ROS, reactive oxygen species; SOD, superoxide dismutase; GSSG, oxidized glutathione; 4-HNE, 4-hydroxynonenal; ELISA, enzyme-linked immunosorbent assay (Image courtesy of Graphpad Prism 9.0.0).

via tail vein twice weekly for 12 weeks; model group: Fed high-fat chow (D12108C; Research Diets, New Brunswick, NJ, USA) and injected with 200 μL saline; NGR-Irisin-LP group: Fed high-fat chow and injected with 200 μL NGR-targeted irisin liposomes (0.01 μg/μL).

Inclusion criteria: Baseline weight 20–25 g, no prior infections. Exclusion criteria: Death prior to endpoint, weight loss >20 %. No animals were excluded. At the experiment endpoint, mice were euthanized via intraperitoneal injection of 0.1 % pentobarbital sodium. Aortic tissue and serum were collected for analysis.

Blood Lipid Index Detection

Frozen mouse serum samples were taken out of the –80 °C cryogenic refrigerator in advance and placed in a refrigerator at 4 °C for 12 h. Extracts, standards, working solutions and other reagents were prepared according to the instruction manual, with reference to the reagent kits for TC (BC1980; Solarbio, Beijing, China), TG (BC0620; Solarbio, Beijing, China), low-density lipoprotein cholesterol (LDL-C) (E-BC-K221-M; Elabscience, Wuhan, China), high-density lipoprotein cholesterol (HDL-C) (E-BC-K205-M; Elabscience, Wuhan, China), ox-LDL (E-EL-M0066c; Elabscience, Wuhan, China) of the kit instructions, and finally, the OD value of each well was mea-

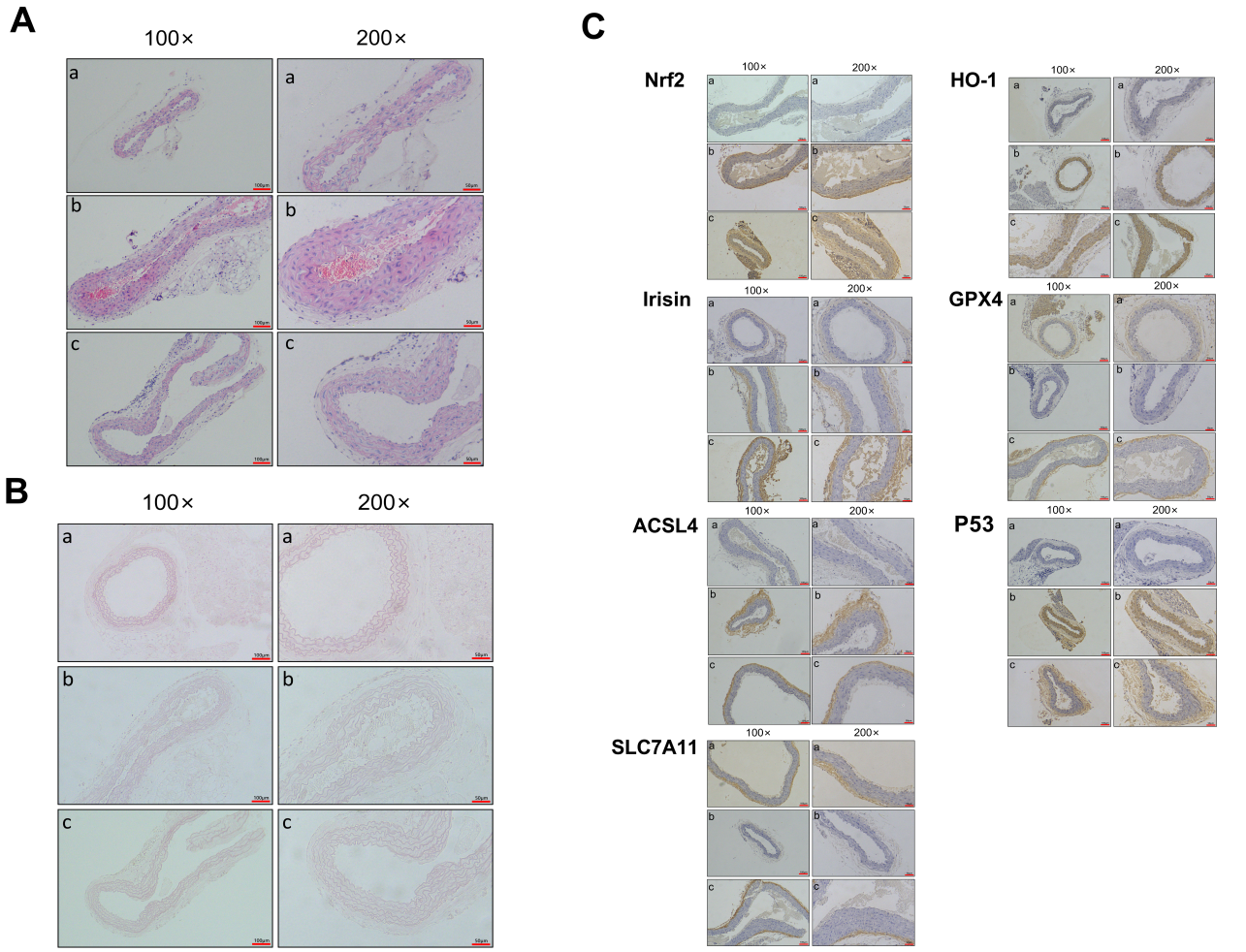

Fig. 6. The pathology of irisin liposomes in carotid artery tissues of mice with atherosclerosis (Scale bars are 50 μm and 100 μm). (**A**) H&E staining was used to detect pathology in carotid artery tissue (n = 6). (**B**) Alizarin red staining was used to detect calcification of aortic tissues (n = 6). (**C**) Immunohistochemistry was performed to detect the expression of genes related to the Nrf2/HO-1 axis in the carotid artery tissues (n = 6). In the picture, a: blank group; b: model group; c: NGR-Irisin-LP. H&E, hematoxylin and eosin (Image courtesy of GraphPad Prism 9.0.0).

sured at 450 nm wavelength by Microplate Reader (Multiskan 51119000; ThermoFisher, Waltham, MA, USA).

Enzyme-Linked Immunosorbent Assay (ELISA) and Colorimetric Methods

Serum from the mice was collected and centrifuged at 1000 g for 20 min, and the supernatant was collected. The assays were performed according to the protocols of the manufacturers of Fe^{2+}(BC5415; Solarbio, Beijing, China), malondialdehyde (MDA) (BC0020; Solarbio, Beijing, China), glutathione (GSH) (BC1170; Solarbio, Beijing, China), ROS (YFXEM00584; Yfxbio, Beijing, China), superoxide dismutase (SOD) (BC0175; Solarbio, Beijing, China), oxidized glutathione (GSSG) (BC1180; Solarbio, Beijing, China), 4-hydroxynonenal (4-HNE) (E-EL-0128c; Elabscience, Wuhan, China), irisin (E-EL-M2743c; Elabscience, Wuhan, China), Nrf2 (E-EL-M2607c; Elabscience, Wuhan, China), HO-1 (ml001855; Mlbio, Shanghai, China), GPX4 (JL46273; Shanghai Jianglai Biotechnology Co., Ltd., Shanghai, China), ACSL4 (SED674Mu; Cloud-Clone Corp, Wuhan, China), P53 (SEA928Mu; Cloud-Clone Corp, Wuhan, China) and SLC7A11 (JL52009, Shanghai Jianglai Biotechnology Co., Ltd., Shanghai, China) assay kits. The OD value of each well was measured by Microplate Reader (Multiskan 51119000, ThermoFisher, Waltham, MA, USA).

Hematoxylin and Eosin (H&E) Staining and Alizarin Red Staining

The samples were fixed in formalin and dehydrated using an alcohol gradient. After paraffin embedding, the specimens were sectioned at a thickness of 5 μm. The prepared sections were then heated at 60 °C for 2 h. The samples were then removed from the oven. A portion of the sec-

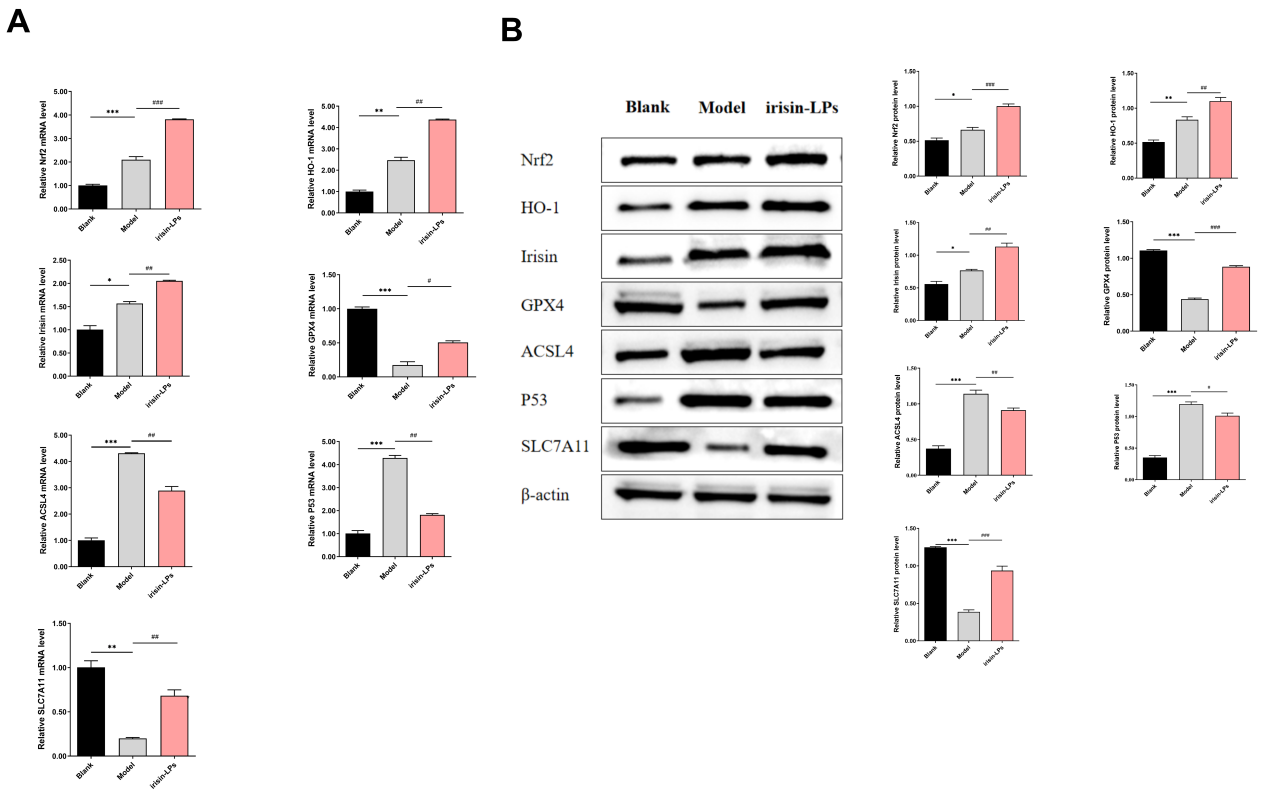

Fig. 7. Investigate the activation of Nrf2/HO-1 signaling pathway by irisin liposomes in an atherosclerosis mouse model. (**A**) qRT-PCR was performed to detect the mRNA expression level of *Nrf2/HO-1* axis-related genes in carotid artery tissues (n = 6). (**B**) Western blot was performed to detect the protein expression level of Nrf2/HO-1 axis-related genes in carotid artery tissues (n = 6). Based on blank group, $^{*}p < 0.05$, $^{**}p < 0.01$, $^{***}p < 0.001$; based on model group, $^{\#}p < 0.05$, $^{\#\#}p < 0.01$, $^{\#\#\#}p < 0.001$ (Image courtesy of GraphPad Prism 9.0.0).

tions was removed from the oven, cooled at room temperature, dewaxed, and dehydrated. The sections were stained with hematoxylin and 0.5 % eosin (G1140; Solarbio, Beijing, China), washed, dehydrated, and air-dried. Drops of neutral gel were added and the lids were sealed. A portion of the sections was stained with alizarin red staining solution and subjected to separate baking and sealing procedures. The sections were observed under a microscope (BX51; Olympus, Tokyo, Japan) and five random fields of view were collected.

Immunohistochemistry

The carotid artery tissues were fixed in 10 % neutral formalin, dehydrated in gradient alcohol, embedded in wax blocks, and sectioned using a microtome (RM2235; Leica, Nussloch, Germany). Subsequently, the wax blocks were individually dewaxed, antigenically repaired using sodium citrate and goat serum, and incubated at 4 °C with the following primary antibodies: irisin (Abcam, ab181884; Cambridge, MA, USA), Nrf2 (Abcam, ab31163; Cambridge, MA, USA), HO-1 (Abcam, ab189491; Cambridge, MA, USA), GPX4 (Abcam, ab125066; Cambridge, MA, USA), ACSL4 (Abcam, ab155282; Cambridge, MA, USA), P53 (Abcam, ab131442; Cambridge, MA, USA), and SLC7A11 (Abcam, ab307601; Cambridge, MA, USA), and incubated with goat anti-rabbit immunoglobulin G (IgG) (Abcam, ab6721; Cambridge, MA, USA) and goat anti-mouse IgG (Abcam, ab6728; 30 min, Cambridge, MA, USA). Staining was performed using 3,3′-diaminobenzidine (DAB) (DA1010; Solarbio, Beijing, China) and hematoxylin (G1140; Solarbio, Beijing, China). Stained paraffin sections were photographed under a light microscope (BX51; Olympus, Tokyo, Japan), five random fields of view were selected for each sample, and the average optical density of the sections was analyzed semi-quantitatively using ImageJ software (version 1.8.0; NIH, Bethesda, MD, USA).

Blinding

Group allocation: Investigators administering injections and collecting tissues were aware of group assignments. Outcome assessment: Pathologists performing H&E staining, immunohistochemistry, and biochemical assays (ELISA, qRT-PCR) were blinded to group identities. Statisticians analyzed coded data without knowledge of group labels until final statistical interpretation.

Toxicity and Biocompatibility Assessment

At the experimental endpoint, blood samples were collected via cardiac puncture. Serum was isolated by centrifugation (3000 rpm, 10 min). Alanine aminotransferase (ALT), aspartate aminotransferase (AST), blood urea nitrogen (BUN), and creatinine (Cr) levels were measured using commercially available kits (Nanjing Jiancheng Bioengineering Institute, Nanjing, China; Batch No. for ALT kit, AST kit, BUN kit and Cr kit: C009-2-1, C010-2-1, C013-2-1 and C011-2-1). The test results are shown in **Supplementary Table 1**.

Data Analysis and Statistics

Data expressed as mean ± SD. Inter-group comparisons utilized unpaired *t*-tests, Mann-Whitney U, or chi-square tests, while multi-group analyses employed one-way analysis of variance (ANOVA) or Kruskal-Wallis with post hoc testing. Normality was tested using Shapiro-Wilk test. Values of $p < 0.05$ were considered to indicate a statistically significant difference. *p*-values were adjusted using Bonferroni correction where applicable. Statistical analyses were conducted using SPSS 26.0 (IBM, Armonk, CA, USA), with experiments independently replicated in triplicate to ensure reproducibility.

Results

Successful Construction of Liposome-Encapsulated Irisin and Exploration of the Appropriate Irisin Concentration

The particle size of the liposomes was observed using scanning electron microscopy, and the liposomes were spherical in shape with folds on the surface and a sphere radius of approximately 1 μm (Fig. 1**A**). The encapsulation rate of irisin was calculated by lysing the irisin liposomes, and it was found that the encapsulation rate of irisin reached more than eighty-five percent for all concentrations (Fig. 1**B**). The CCK-8 assay was used to detect that umbilical vein endothelial cell viability peaked at 25 nmol/L, as measured by CCK-8 assay, and this concentration was selected for subsequent experiments (Fig. 1**C**).

Irisin Liposomes Show Better Amelioration of Vascular Endothelial Cell Injury Models

Compared to the model and irisin groups, the mitochondrial membrane cristae and outer membrane structures were intact, and membrane density was restored in the NGR-Irisin-LP group (Fig. 2**A**). By detecting the mitochondrial membrane potential, the NGR-Irisin-LP group had a lower mitochondrial membrane potential rate (Fig. 2**B**). The results of the LDH assay showed that the NGR-Irisin-LP group had significantly reduced cellular toxicity compared to the model group and the irisin group (Fig. 2**C**), and the NGR-Irisin-LP group had a lower apoptosis rate compared to the model group and the irisin group (Fig. 2**D**).

Table 1. Primer sequences for qRT-PCR.

Primers	Sequences (5′–3′)
Nrf2	
F	ACACGGTCCACAGCTCATC
R	TGTCAATCAAATCCATGTCCTG
HO-1	
F	CTCAACATCCAGCTCTTTGAG
R	AATCTTGCACTTTGTTGCTGGC
Irisin	
F	GTCTCCCACCACCATCTT
R	TCTGTCTCTGAGTGTAGCCTTAGC
GPX4	
F	AGGCAAGACCGAAGTAAACTACAC
R	TCTCTTCGTTACTCCCTGGCT
ACSL4	
F	CCGACCTAAGGGAGTGATGA
R	CCTGCAGCCATAGGTAAAGC
P53	
F	CGTGTGGAGTATTTGGATG
R	GTAGTTGTAGTGGATGGTGGT
SLC7A11	
F	ATCTGCTTCATCGCCTACTT
R	TCTCTGCCTCTGGTAAAAAC
GAPDH	
F	GATGACATCAAGAAGGTGGTG
R	GTCATACCAGGAAATGAGCTTG

qRT-PCR, quantitative real-time polymerase chain reaction; *Nrf2*, nuclear factor erythroid 2-related factor 2; *HO-1*, heme oxygenase-1; *GPX4*, glutathione peroxidase 4; *ACSL4*, acyl-CoA synthetase long chain family member 4; *P53*, tumor protein 53; *SLC7A11*, solute carrier family 7 member 11; *GAPDH*, glyceraldehyde 3-phosphate dehydrogenase.

Irisin Activates the Nrf2/HO-1 Signaling Pathway in Injured Vascular Endothelial Cells

It was verified by qRT-PCR and western blotting that the Nrf2/HO-1 signaling pathway was activated after irisin treatment, and the expression levels of Nrf2, HO-1, GPX4, and SLC7A11 were significantly upregulated in the NGR-Irisin-LP group, and irisin, ACSL4, and p53 were significantly downregulated in the NGR-Irisin-LP group, when compared with the model group and the irisin group (Fig. 3**A,B**).

Downregulation of Lipid Indices by Irisin Liposomes

Atherosclerosis modeling was established by feeding high-fat chow to *ApoE*$^{-/-}$ mice, and the body weight of mice in the model group was significantly higher than that of the blank group (Fig. 4**A**). Compared with the model group, the NGR-Irisin-LP group significantly downregulated the levels of TC, TG, LDL-C, and ox-LDL, and significantly upregulated the expression level of HDL-C (Fig. 4**B**).

Irisin Liposomes Inhibited Ferroptosis in a Mouse Model of Atherosclerosis

Compared with the model group, the NGR-Irisin-LP group showed significantly downregulated levels of Fe^{2+}, MDA, ROS, GSSG, and 4-HNE associated with ferroptosis, and significantly upregulated levels of GSH and SOD associated with antioxidants in the carotid artery tissues of atherosclerotic mice (Fig. 5**A–D**). Meanwhile, the NGR-Irisin-LP group showed significantly upregulated levels of irisin, Nrf2, HO-1, GPX4, and SLC7A11 and significantly downregulated levels of ACSL4 and P53 in carotid artery tissues of atherosclerotic mice, compared with the model group (Fig. 5**E**).

Irisin Liposomes Improved Carotid Artery Tissue Pathology in Atherosclerotic Mice

H&E staining results showed that the carotid artery tissue structure was normal in the blank group, and lipid accumulation and plaque area were significantly increased in the model group (Fig. 6**A**). Compared with the model group, the NGR-Irisin-LP group showed ameliorated vascular pathology in the carotid artery tissue of atherosclerotic mice (Fig. 7**A**). Calcium salt deposits in the tissues stained red or orange-red, with no obvious red color in the carotid arteries of the blank group and a more obvious red color in the model group, while the red color in the carotid artery tissues of the NGR-Irisin-LP group was significantly reduced compared with that of the model group (Fig. 6**B**). The immunohistochemistry (IHC) results showed that the expression levels of irisin, Nrf2, HO-1, GPX4, and SLC7A11 were significantly up-regulated, and the expression levels of ACSL4 and P53 were significantly down-regulated in carotid artery tissues in the NGR-Irisin-LP group compared with the model group (Fig. 6**C**).

Irisin Liposomes Activate the Nrf2/HO-1 Signaling Pathway in Mouse Models of Atherosclerosis

The results of qRT-PCR and western blotting showed that compared with the model group, the NGR-Irisin-LP group had significantly upregulated protein and messenger RNA (mRNA) expression levels of irisin, Nrf2, HO-1, GPX4, and SLC7A11, and significantly downregulated protein and mRNA expression levels of ACSL4 and P53 (Fig. 7**A,B**).

Discussion

Recent studies have shown that ferroptosis in vascular endothelial cells plays an important role in the progression of atherosclerosis [33,34]. It has been found that iron levels are significantly higher in clinically diagnosed coronary atherosclerotic arterial tissues than in healthy arterial tissues, and that iron overload promotes oxidative stress and inflammatory responses in cells [33,34]. Pathological analysis of human coronary arteries revealed that the severity of atherosclerosis was positively correlated with the expression of ACSL4 and negatively correlated with the expression of GPX4 [35]. The oxidation of unsaturated fatty acids to harmful lipid peroxides damages endothelial cells, and the inhibition of ferroptosis can reduce ox-LDL-induced endothelial cell damage and alleviate atherosclerosis. Fer-1, an inhibitor of ferroptosis, significantly increased the viability of ox-LDL-treated cells, reduced intracellular iron accumulation, effectively attenuated endothelial cell damage, and inhibited lipid peroxidation [27].

Skeletal muscle is a major source of irisin, and elevated serum irisin levels after exercise promote the conversion of white fat to brown fat, which promotes thermogenesis [10]. Available studies suggest that reduced irisin levels are a risk factor for carotid intima-media thickening, and that higher irisin serum levels are associated with lower coronary artery calcification and myocardial infarction [36, 37]. Irisin improved the function of vascular endothelial cells, reduced the level of inflammatory factors in the blood, and alleviated carotid atherosclerosis in $ApoE^{-/-}$ mice by up-regulating the expression of miR-126-5p [38]. Irisin increased the viability, migration, and angiogenesis of ox-LDL-treated endothelial cells and decreased apoptosis, inflammatory cytokines, and intracellular reactive oxygen species (ROS) levels [39]. Irisin also reduces oxidative stress and apoptosis in human umbilical vein endothelial cells by inhibiting protein kinase C beta isoform (PKC-β)/reduced nicotinamide adenine dinucleotide phosphate (NADPH) oxidase and nuclear factor kappa B (NF-κB)-inducible nitric oxide synthase (iNOS) pathway, which in turn reduces oxidative stress and apoptosis in human umbilical vein endothelial cells [15]. These findings suggest that exogenous irisin may play a role in ameliorating atherosclerosis by improving lipid metabolism and inhibiting lipid peroxidation. In this study, we enhanced the stability and bioavailability of irisin using liposome-encapsulated irisin. The results showed that liposome-encapsulated irisin had a better amelioration of atherosclerosis.

In this study, irisin liposomes were successfully prepared using a complex emulsion method. The viability of the HUVEC cell line was better at an irisin concentration of 25 nmol/L using the CCK-8 kit. By constructing a vascular endothelial cell injury model, we found that the apoptosis rate was significantly decreased in the irisin liposome group. The LDH cytotoxicity assay showed that the irisin liposomes group also had a lower concentration of LDH, indicating higher cell survival and a protective effect of irisin liposomes on vascular endothelial cells. The expression of ferroptosis-related genes in vascular endothelial cells was detected by western blotting and qRT-PCR, and the results showed that irisin liposomes upregulated the expression levels of Nrf2, HO-1, GPX4, and SLC7A11, while downregulating the expression of ACSL4, P53, and irisin, as compared with the model group. In the follow-up experiments, we successfully constructed an atherosclerosis mouse model with irisin liposome adminis-

tration, which not only reduced the level of harmful lipoproteins in serum, but also lowered the level of indices related to the occurrence of ferroptosis and elevated the level of antioxidant indexes, suggesting that exogenous irisin can inhibit atherosclerosis by improving lipid metabolism and inhibiting lipid peroxidation. One limitation of our study is the lack of direct evidence for *in vivo* targeting of NGR-modified liposomes. Future studies incorporating fluorescent labeling and imaging could help confirm tissue-specific accumulation. The results of H&E staining, alizarin red staining, and immunohistochemistry showed that irisin liposomes significantly ameliorated the pathology in the carotid artery tissues of atherosclerotic mice, mainly through the activation of the Nrf2/HO-1 signaling pathway. A previous study has shown that irisin rescues diabetic myocardial microvessels from oxidative stress and apoptosis via the ERK1/2/Nrf2/HO-1 pathway [40]. The antioxidant and anti-apoptotic effects of irisin have been extensively studied [41,42].

In the present study, we focused on the role and mechanism of irisin in resisting ferroptosis. This study confirmed that irisin encapsulated by liposomes can exert a stronger therapeutic effect on atherosclerosis.

Conclusions

Irisin liposomes had a better protective effect on vascular endothelial cells, inhibited ferroptosis by activating the Nrf2/HO-1 signaling pathway, and ameliorated damage in a mouse model of AS, which had a therapeutic effect on AS.

List of Abbreviations

AS, atherosclerosis; CVD, cardiovascular disease; LDL-C, low-density lipoprotein cholesterol; HDL-C, high-density lipoprotein cholesterol; TC, total cholesterol; TG, triglyceride; ox-LDL, oxidized low-density lipoprotein; ROS, reactive oxygen species; MDA, malondialdehyde; GSH, glutathione; GSSG, oxidized glutathione; SOD, superoxide dismutase; 4-HNE, 4-hydroxynonenal; H&E, hematoxylin and eosin; IHC, immunohistochemistry; qRT-PCR, quantitative real-time polymerase chain reaction; Nrf2, nuclear factor erythroid 2-related factor 2; HO-1, heme oxygenase-1; GPX4, glutathione peroxidase 4; ACSL4, acyl-CoA synthetase long chain family member 4; SLC7A11, solute carrier family 7 member 11; P53, tumor protein 53; HUVEC, human umbilical vein endothelial cell; CCK-8, Cell Counting Kit-8; LDH, lactate dehydrogenase; DMSO, dimethyl sulfoxide; STR, short tandem repeat; PBS, phosphate-buffered saline; OD, optical density; LPs, liposomes and particles; NGR, Asn-Gly-Arg peptide (targeting sequence); DAB, 3,3′-diaminobenzidine; GAPDH, glyceraldehyde 3-phosphate dehydrogenase; ALT, alanine aminotransferase; AST, aspartate aminotransferase; BUN, blood urea nitrogen; PGC-1α, peroxisome proliferator-activated receptor gamma coactivator 1-alpha; FNDC5, fibronectin type III domain-containing protein 5; UCP1, uncoupling protein 1; ERK, extracellular signal-regulated kinase; NF-κB, nuclear factor kappa B; iNOS, inducible nitric oxide synthase; FBS, fetal bovine serum; Fer-1, ferretin-1; Irisin-LP, irisin liposomes; ELISA, enzyme-linked immunosorbent assay; JC-1, 5,5′,6,6′-tetrachloro-1,1′,3,3′-tetraethylbenzimidazolyl-carbocyanine iodide; cDNA, complementary DNA; mRNA, messenger RNA; IgG, immunoglobulin G; W, aqueous; O, organic; DSPE-mPEG2000-COOH, 1,2-distearoyl-sn-glycero-3-phosphoethanolamine-N-[methoxy(polyethylene glycol)-2000]-carboxylic acid.

Availability of Data and Materials

The datasets used or analyzed during the current study are available from the corresponding author on reasonable request.

Author Contributions

ZH, YRL and QLC contributed to the design of this work and drafted the work. ZH and YRL contributed to the interpretation of data. ZH, YRL and BY analyzed the data. QLC and BY revised critically for important intellectual content. All authors read and approved the final manuscript. All authors agreed to be accountable for all aspects of the work in ensuring that questions related to the accuracy or integrity of any part of the work were appropriately investigated and resolved.

Ethics Approval and Consent to Participate

The study was approved by the Institutional Animal Care and Use Committee of Hebei University (Baoding, China, approval no. 20240301) and performed in accordance with the Guidelines for the Care and Use of Laboratory Animals of Hebei University.

Acknowledgments

Not applicable.

Funding

No funding was received.

Conflict of Interest

The authors declare that they have no competing interests.

Supplementary Material

Supplementary material associated with this article can be found, in the online version, at https://doi.org/10.22203/eCM.v054a02.

References

[1] Goldsborough E 3rd, Osuji N, Blaha MJ. Assessment of Cardiovascular Disease Risk: A 2022 Update. Endocrinology and Metabolism

Clinics of North America. 2022; 51: 483–509. https://doi.org/10.1016/j.ecl.2022.02.005.

[2] World Health Organization. Cardiovascular diseases (CVDs). 2021. Available at: https://www.who.int/news-room/fact-sheets/detail/cardiovascular-diseases-(cvds) (Accessed: 26 June 2025).

[3] Kobiyama K, Ley K. Atherosclerosis. Circulation Research. 2018; 123: 1118–1120. https://doi.org/10.1161/CIRCRESAHA.118.313816.

[4] Deprince A, Haas JT, Staels B. Dysregulated lipid metabolism links NAFLD to cardiovascular disease. Molecular Metabolism. 2020; 42: 101092. https://doi.org/10.1016/j.molmet.2020.101092.

[5] Ballard-Hernandez J, Sall J. Dyslipidemia Update. The Nursing Clinics of North America. 2023; 58: 295–308. https://doi.org/10.1016/j.cnur.2023.05.002.

[6] Lordan R, Tsoupras A, Zabetakis I. Platelet activation and prothrombotic mediators at the nexus of inflammation and atherosclerosis: Potential role of antiplatelet agents. Blood Reviews. 2021; 45: 100694. https://doi.org/10.1016/j.blre.2020.100694.

[7] Kim H, Wrann CD, Jedrychowski M, Vidoni S, Kitase Y, Nagano K, *et al*. Irisin Mediates Effects on Bone and Fat via αV Integrin Receptors. Cell. 2018; 175: 1756–1768.e17. https://doi.org/10.1016/j.cell.2018.10.025.

[8] Zhang Y, Zhang X, Lin S. Irisin: A bridge between exercise and neurological diseases. Heliyon. 2022; 8: e12352. https://doi.org/10.1016/j.heliyon.2022.e12352.

[9] Wrann CD, White JP, Salogiannnis J, Laznik-Bogoslavski D, Wu J, Ma D, *et al*. Exercise induces hippocampal BDNF through a PGC-1α/FNDC5 pathway. Cell Metabolism. 2013; 18: 649–659. https://doi.org/10.1016/j.cmet.2013.09.008.

[10] Boström P, Wu J, Jedrychowski MP, Korde A, Ye L, Lo JC, *et al*. A PGC1-α-dependent myokine that drives brown-fat-like development of white fat and thermogenesis. Nature. 2012; 481: 463–468. https://doi.org/10.1038/nature10777.

[11] Zhang Y, Xie C, Wang H, Foss RM, Clare M, George EV, *et al*. Irisin exerts dual effects on browning and adipogenesis of human white adipocytes. American Journal of Physiology. Endocrinology and Metabolism. 2016; 311: E530–E541. https://doi.org/10.1152/ajpendo.00094.2016.

[12] Cheng ZB, Huang L, Xiao X, Sun JX, Zou ZK, Jiang JF, *et al*. Irisin in atherosclerosis. Clinica Chimica Acta; International Journal of Clinical Chemistry. 2021; 522: 158–166. https://doi.org/10.1016/j.cca.2021.08.022.

[13] Remuzgo-Martínez S, Rueda-Gotor J, Pulito-Cueto V, López-Mejías R, Corrales A, Lera-Gómez L, *et al*. Irisin as a Novel Biomarker of Subclinical Atherosclerosis, Cardiovascular Risk and Severe Disease in Axial Spondyloarthritis. Frontiers in Immunology. 2022; 13: 894171. https://doi.org/10.3389/fimmu.2022.894171.

[14] Zang YH, Chen D, Zhou B, Chen AD, Wang JJ, Gao XY, *et al*. FNDC5 inhibits foam cell formation and monocyte adhesion in vascular smooth muscle cells via suppressing NFκB-mediated NLRP3 upregulation. Vascular Pharmacology. 2019; 121: 106579. https://doi.org/10.1016/j.vph.2019.106579.

[15] Zhu D, Wang H, Zhang J, Zhang X, Xin C, Zhang F, *et al*. Irisin improves endothelial function in type 2 diabetes through reducing oxidative/nitrative stresses. Journal of Molecular and Cellular Cardiology. 2015; 87: 138–147. https://doi.org/10.1016/j.yjmcc.2015.07.015.

[16] Zhang Y, Mu Q, Zhou Z, Song H, Zhang Y, Wu F, *et al*. Protective Effect of Irisin on Atherosclerosis via Suppressing Oxidized Low Density Lipoprotein Induced Vascular Inflammation and Endothelial Dysfunction. PloS One. 2016; 11: e0158038. https://doi.org/10.1371/journal.pone.0158038.

[17] Cheraghi M, Negahdari B, Daraee H, Eatemadi A. Heart targeted nanoliposomal/nanoparticles drug delivery: An updated review. Biomedicine & Pharmacotherapy = Biomédecine & Pharmacothérapie. 2017; 86: 316–323. https://doi.org/10.1016/j.biopha.2016.12.009.

[18] Farjadian F, Ghasemi A, Gohari O, Roointan A, Karimi M, Hamblin MR. Nanopharmaceuticals and nanomedicines currently on the market: challenges and opportunities. Nanomedicine. 2019; 14: 93–126. https://doi.org/10.2217/nnm-2018-0120.

[19] Shah S, Dhawan V, Holm R, Nagarsenker MS, Perrie Y. Liposomes: Advancements and innovation in the manufacturing process. Advanced Drug Delivery Reviews. 2020; 154–155: 102–122. https://doi.org/10.1016/j.addr.2020.07.002.

[20] Kattoor AJ, Pothineni NVK, Palagiri D, Mehta JL. Oxidative Stress in Atherosclerosis. Current Atherosclerosis Reports. 2017; 19: 42. https://doi.org/10.1007/s11883-017-0678-6.

[21] Zheng D, Liu J, Piao H, Zhu Z, Wei R, Liu K. ROS-triggered endothelial cell death mechanisms: Focus on pyroptosis, parthanatos, and ferroptosis. Frontiers in Immunology. 2022; 13: 1039241. https://doi.org/10.3389/fimmu.2022.1039241.

[22] Lubrano V, Balzan S. LOX-1 and ROS, inseparable factors in the process of endothelial damage. Free Radical Research. 2014; 48: 841–848. https://doi.org/10.3109/10715762.2014.929122.

[23] Batty M, Bennett MR, Yu E. The Role of Oxidative Stress in Atherosclerosis. Cells. 2022; 11: 3843. https://doi.org/10.3390/cells11233843.

[24] Sun HJ, Zhao MX, Ren XS, Liu TY, Chen Q, Li YH, *et al*. Salusin-β Promotes Vascular Smooth Muscle Cell Migration and Intimal Hyperplasia After Vascular Injury via ROS/NFκB/MMP-9 Pathway. Antioxidants & Redox Signaling. 2016; 24: 1045–1057. https://doi.org/10.1089/ars.2015.6475.

[25] Galaris D, Barbouti A, Pantopoulos K. Iron homeostasis and oxidative stress: An intimate relationship. Biochimica et Biophysica Acta. Molecular Cell Research. 2019; 1866: 118535. https://doi.org/10.1016/j.bbamcr.2019.118535.

[26] Jiang X, Stockwell BR, Conrad M. Ferroptosis: mechanisms, biology and role in disease. Nature Reviews. Molecular Cell Biology. 2021; 22: 266–282. https://doi.org/10.1038/s41580-020-00324-8.

[27] Bai T, Li M, Liu Y, Qiao Z, Wang Z. Inhibition of ferroptosis alleviates atherosclerosis through attenuating lipid peroxidation and endothelial dysfunction in mouse aortic endothelial cell. Free Radical Biology & Medicine. 2020; 160: 92–102. https://doi.org/10.1016/j.freeradbiomed.2020.07.026.

[28] Loboda A, Damulewicz M, Pyza E, Jozkowicz A, Dulak J. Role of Nrf2/HO-1 system in development, oxidative stress response and diseases: an evolutionarily conserved mechanism. Cellular and Molecular Life Sciences: CMLS. 2016; 73: 3221–3247. https://doi.org/10.1007/s00018-016-2223-0.

[29] Ma Q. Role of nrf2 in oxidative stress and toxicity. Annual Review of Pharmacology and Toxicology. 2013; 53: 401–426. https://doi.org/10.1146/annurev-pharmtox-011112-140320.

[30] Kishimoto Y, Sasaki K, Saita E, Niki H, Ohmori R, Kondo K, *et al*. Plasma Heme Oxygenase-1 Levels and Carotid Atherosclerosis. Stroke. 2018; 49: 2230–2232. https://doi.org/10.1161/STROKEAHA.118.022256.

[31] Yang R, Gao W, Wang Z, Jian H, Peng L, Yu X, *et al*. Polyphyllin I induced ferroptosis to suppress the progression of hepatocellular carcinoma through activation of the mitochondrial dysfunction via Nrf2/HO-1/GPX4 axis. Phytomedicine: International Journal of Phytotherapy and Phytopharmacology. 2024; 122: 155135. https://doi.org/10.1016/j.phymed.2023.155135.

[32] Yang W, Wang Y, Zhang C, Huang Y, Yu J, Shi L, *et al*. Maresin1 Protect Against Ferroptosis-Induced Liver Injury Through ROS Inhibition and Nrf2/HO-1/GPX4 Activation. Frontiers in Pharmacology. 2022; 13: 865689. https://doi.org/10.3389/fphar.2022.865689.

[33] Xu S. Iron and Atherosclerosis: The Link Revisited. Trends in Molecular Medicine. 2019; 25: 659–661. https://doi.org/10.1016/j.molmed.2019.05.012.

[34] Hu X, Cai X, Ma R, Fu W, Zhang C, Du X. Iron-load exacerbates the severity of atherosclerosis via inducing inflammation and enhancing

the glycolysis in macrophages. Journal of Cellular Physiology. 2019; 234: 18792–18800. https://doi.org/10.1002/jcp.28518.

[35] Zhou Y, Zhou H, Hua L, Hou C, Jia Q, Chen J, *et al*. Verification of ferroptosis and pyroptosis and identification of PTGS2 as the hub gene in human coronary artery atherosclerosis. Free Radical Biology & Medicine. 2021; 171: 55–68. https://doi.org/10.1016/j.freeradbiomed.2021.05.009.

[36] Hisamatsu T, Miura K, Arima H, Fujiyoshi A, Kadota A, Kadowaki S, *et al*. Relationship of serum irisin levels to prevalence and progression of coronary artery calcification: a prospective, population-based study. International Journal of Cardiology. 2018; 267: 177–182. https://doi.org/10.1016/j.ijcard.2018.05.075.

[37] Anastasilakis AD, Koulaxis D, Kefala N, Polyzos SA, Upadhyay J, Pagkalidou E, *et al*. Circulating irisin levels are lower in patients with either stable coronary artery disease (CAD) or myocardial infarction (MI) versus healthy controls, whereas follistatin and activin A levels are higher and can discriminate MI from CAD with similar to CK-MB accuracy. Metabolism: Clinical and Experimental. 2017; 73: 1–8. https://doi.org/10.1016/j.metabol.2017.05.002.

[38] Zhang Y, Song H, Zhang Y, Wu F, Mu Q, Jiang M, *et al*. Irisin Inhibits Atherosclerosis by Promoting Endothelial Proliferation Through microRNA126-5p. Journal of the American Heart Association. 2016; 5: e004031. https://doi.org/10.1161/JAHA.116.004031.

[39] Zhang M, Xu Y, Jiang L. Irisin attenuates oxidized low-density lipoprotein impaired angiogenesis through AKT/mTOR/S6K1/Nrf2 pathway. Journal of Cellular Physiology. 2019; 234: 18951–18962. https://doi.org/10.1002/jcp.28535.

[40] Zhu D, Zhang X, Wang F, Ye Q, Yang C, Liu D. Irisin rescues diabetic cardiac microvascular injury via ERK1/2/Nrf2/HO-1 mediated inhibition of oxidative stress. Diabetes Research and Clinical Practice. 2022; 183: 109170. https://doi.org/10.1016/j.diabres.2021.109170.

[41] Li DJ, Li YH, Yuan HB, Qu LF, Wang P. The novel exercise-induced hormone irisin protects against neuronal injury via activation of the Akt and ERK1/2 signaling pathways and contributes to the neuroprotection of physical exercise in cerebral ischemia. Metabolism: Clinical and Experimental. 2017; 68: 31–42. https://doi.org/10.1016/j.metabol.2016.12.003.

[42] Wang Y, Tian M, Tan J, Pei X, Lu C, Xin Y, *et al*. Irisin ameliorates neuroinflammation and neuronal apoptosis through integrin $\alpha V\beta 5$/AMPK signaling pathway after intracerebral hemorrhage in mice. Journal of Neuroinflammation. 2022; 19: 82. https://doi.org/10.1186/s12974-022-02438-6.

Editor's note: The Scientific Editor responsible for this paper was Bo Lei.

Received: 25th March 2025; **Accepted**: 18th July 2025; **Published**: 28th November 2025